Numerical Modelling of a Tidal Turbine Behaviour under Realistic Unsteady Tidal Flow

T. Leroux[#1], N. Osbourne[#2], J.M. McMillan[*3], D. Groulx[#4], A.E. Hay[*5]

[#]*Department of Mechanical Engineering, Dalhousie University*
Halifax, Nova Scotia, Canada

[1]tn876184@dal.ca

[2]nick.a.osbourne@dal.ca

[4]dominic.groulx@dal.ca

[*] *Department of Oceanography, Dalhousie University*

[3]justine.mcmillan@dal.ca

[5]alex.hay@dal.ca

***Abstract*— This paper presents the results of three dimensional numerical simulations of a three-bladed horizontal axis tidal turbine (HATT) under realistic turbulent tidal flow conditions. All results provided incorporate the Reynolds-averaged Navier-Stokes (RANS) Shear Stress Transport (SST) turbulence model. Simulations cover a range of tip speed ratios (TSR = 3 – 4.5) and flow velocities (1.6, 1.8 and 2.05 m/s) at a fixed hub pitch angle of approximately 28°. Simulations are performed at a time-dependent, turbulent inflow velocity based on measurements obtained in Grand Passage, Nova Scotia. Thrust and power coefficients are compared to numerical results obtained in steady flow for validation purposes. The results show a good level of agreement between steady and transient simulations. Results of a power production comparison show a small reduction in power production (4%), when comparing turbine operation in a realistic unsteady tidal flow to operation in a steady flow. Near field and far field wake propagation is also investigated and compared to the wake obtained with a steady flow.**

***Keywords*— Computational Fluid Dynamics (CFD), Horizontal Axis Tidal Turbine (HATT), Transient Simulations, Reynolds-averaged Navier-Stokes (RANS), Real Tidal Flow Inlet Conditions**

I. Introduction

General concerns of global warming, along with the cost of fossil fuels, are rising. As a consequence, increasing focus is put on the development of renewable energy industries. Some of these industries, such as hydroelectricity or on-shore wind, are well established. On the other hand, marine energy sources are not yet exploited.

Unlike on-shore wind industries, marine energy industries are facing new challenges due to the harsher conditions of the environment in which they operate. Oceans present their own physical challenges that make development, manufacturing and marine energy device maintenance difficult and costly. These challenges include: salinity, high turbulence levels, rapid tidal flow, environmental issues and poor accessibility. It is nevertheless believed that the outcome is worth the effort.

It has been estimated that tidal stream energy capacity could exceed 120 GW globally [1]. Although extracting this total power is not technically feasible, it is estimated by many sources that 75 to 90 GW can be extracted with the different existing technologies [2].

In marine energy industries, particularly in-stream tidal, reliability will be the key. Turbine developers are putting more and more emphasis on pre-deployment testing in order to garner meaningful information on the performance of tidal turbines.

As stated by tidal turbine manufacturers, measuring the performance of a tidal turbine presents two key challenges to the tidal energy industry: 1) prediction in the design stage and 2) verification of the performance once operational [3]. Prediction in the design stage is currently done through small-scale steady-state experimental testing, which uses constant velocity towing tanks [4, 5] or flume tanks [6] to determine power produced and thrust acting on the designed turbine; or a numerical model of the turbine, using constant inlet velocity conditions, over which the flow is simulated using either a simpler blade element/momentum (BEM) [7, 8] method, actuator disks representations [9] or the more powerful and accurate computational fluid dynamics (CFD) methods [10].

These tools have been, and continue to be, used for tidal turbine design, optimization and characterization, easily providing numerous and repeatable data. But recent results presented by Dr. Bjorn Elsaesser's group from Queen's University Belfast showed that the turbine maximum operating power coefficient (C_p) was reduced by 24%, with a consequential reduction in power production of 30%, when comparing turbine operation in a real unsteady tidal flow to steady tests performed by pushing the turbine in still water [11].

The second challenge, verification of the performance once operational, has only been taken on by a select few turbine developers: Alstom through 4 years of careful measurement and testing [3], OpenHydro through years at EMEC [12], and the aforementioned results from the Queen's University group. The latter results point to the fact that most turbine developers, relying on steady tests, might be overestimating their turbine power rating by tens of percent. This could have

an important impact on the overall financial assessment and economic viability of tidal projects. It's therefore important to perform numerical studies using real unsteady velocity conditions to know more precisely the impact of unsteadiness on the turbines performance.

Of the various numerical methods that are employed today for studying turbulent flow over turbines, very few can be employed to study unsteady flow with high enough accuracy. Blade element/momentum (BEM) [7, 8] methods have been shown to be insufficient for unsteady loading [13]. The actuator disc method still lacks the solution quality that would result from a standalone CFD model. A CFD approach has been shown to be capable of resolving turbulence in the near and far field regions at fine resolution for a three dimensional horizontal axis tidal turbine (HATT) [14]. The most commonly used turbulence model in the field of tidal turbine simulation today is the Shear Stress Transport (SST) model. It utilizes k-ω turbulence closure in the inner boundary regions and k-ε closure in the free stream regions, and is capable of resolving turbulence with acceptable margins of error [15, 16].

This shift into unsteady studies has started recently with numerous papers in the last two years looking at various engineering aspects, for example: CFD study of the load on turbine blades stemming from unsteady tidal flow [17], experimental study in a circulating tank of unsteady turbulence (generated artificially using static grids) effect on a small-scale tidal turbine [6, 18, 19]; these studies however used randomly generated flow field and turbulence level. Only one recent conference paper from a team at the University of Manchester (UK) shows the integration of "real tidal" velocity data as the inlet condition of a CFD simulation to properly study the impact of unsteadiness in the flow, in this case using data from the EMEC test site in the Orkney Isles [16].

In Canada, work on characterizing the unsteadiness of tidal flows in the Bay of Fundy has been underway for a few years [20]. Several measurements campaigns have taken place in Grand Passage, Nova Scotia [20, 21, 22]; where it has been demonstrated that standard commercially-available ADCPs can be used to obtain representative estimates of second-order turbulence statistics, including the turbulent kinetic energy and the rate of energy dissipation. High fidelity detached eddy simulations have also been used to characterize the unsteady flow in the Minas Passage [23].

Researchers at Dalhousie University are well positioned to study the impact of unsteady flow on turbine performance using a recently developed CFD model [24]. The numerical methodology was validated against experimental results [4] and used to study turbine wake characteristics [24]. In this paper, the inlet conditions are established based on measurements obtained in Grand Passage, Nova Scotia. The turbine performance and wake dynamics are assessed for a variety of mean flow speeds and tip speed ratios, and comparisons to steady flow simulations are made.

II. Turbine Geometry

The turbine geometry was developed to model the experimental turbine used by Doman *et al.* [5]. TABLE I presents the blade geometry which is based on the NREL S814 airfoil; the overall turbine has a diameter of 762 mm. The axis of rotation is located at 25% of the chord from the leading edge for each cross section. The hub pitch angle for the experimental turbine was measured to be 28 ± 0.875°, 28.875° was used in the numerical model. The nacelle and support structure geometries were estimated from reviews of the publications, dimensions of which are provided in TABLE II. The blade roots and rotor hub were greatly simplified from the experimental setup to facilitate meshing (Fig. 1).

III. Numerical Modelling

A. Fluid Domain

The numerical fluid domain length is based on the dimensions of the Kelvin Hydrodynamics Laboratory tow tank at the Strathclyde University where experimental tests for Doman *et al.*'s turbine were conducted [5].

TABLE I
Blade Parameters [5]

Radius (m)	Twist (°)	Chord (m)
0.089	0	0.0643
0.114	-4.38	0.0629
0.149	-10.74	0.0598
0.183	-14.80	0.0560
0.216	-17.33	0.0516
0.251	-18.91	0.0473
0.286	-19.75	0.0426
0.321	-20.39	0.0381
0.355	-20.87	0.0337
0.381	-21.11	0.0249

TABLE II
Nacelle Geometry Dimensions

Parameter	Dimension
Nacelle Length	1700 mm
Nacelle Diameter	150 mm
Rotor depth	700 mm

Fig. 1 Turbine rendering.

TABLE III
TOW TANK PARAMETERS [5]

Parameter	Magnitude
Length	76 m
Breadth	4.6 m
Height	2.5 m
Maximum flow speed	5 m/s

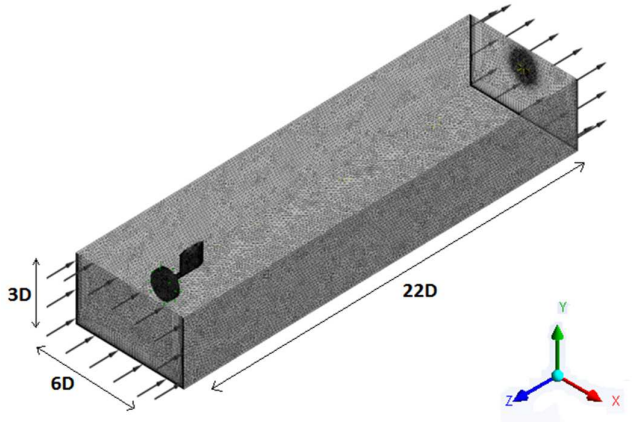

Fig. 2 Fluid domain.

Figure 2 and Table III presents the dimensions of the facility. These parameters are represented in the numerical fluid domain with the exception of the domain length. The domain length was shortened to 22*D*, with inlet and outlet lengths of 2*D* and 20*D* respectively, where D = 762 mm denotes the turbine diameter. The fluid domain is shown in Fig. 2 and the turbine is located at (x, y, z) = (0, 0, 0). It has been shown that this length is sufficient as the near wake physics and performance of the turbine is not significantly affected by the outlet domain length [24].

B. Turbulence Models

The *k-ω* Shear Stress Transport (SST) Reynolds-averaged Navier-Stokes (RANS) turbulence model was chosen to capture turbulent fluctuations in the flow [25]. This is generally accepted as the most suitable turbulence model in similar applications [9, 15, 24]. SST is a two equation eddy viscosity model that employs *k-ω* in the inner boundary layer and transitions to *k-ε* in the free stream. SST thereby negates the poor performance of *k-ε* near solid surfaces and the exaggerated sensitivity of *k-ω* in free-shear flows [9].

C. Computational Mesh

The fluid domain was spatially discretized using ANSYS Mesher. Unstructured tetrahedrals were used to accurately represent the turbine geometry. The domain consisted of a rotating cylindrical domain encompassing the turbine and a larger stationary domain. Continuity across the interface between the two domains was achieved using the General Grid Interface (GGI).

Several parameters of the mesh were tested to ensure the geometry of the turbine was modelled with enough resolution to accurately capture the its performance. These included the minimum and maximum cell size, curvature normal angle on the blade and growth rate. Special attention was paid to the quality of the inflation layers, where the effect of the first layer height and number of layers were tested [28]. This numerical model was then compared to experimental results performed by Doman *et al.* in the Kelvin Hydrodynamics Laboratory tow tank for validation purposes [5, 28]. A good level of agreement between the numerical and experimental results was shown [28].

Figure 3 provides a detailed view of the turbine surface mesh, and Fig. 4 shows the cross-section of the blade mesh.

D. Boundary Conditions

The domain boundary conditions are provided in Table IV. At the inlet (z = -2*D*), a time- and depth-dependent velocity was imposed where the synthetic data was based on ADCP velocity measurements that were obtained in 2013 at the northern end of Grand Passage, Nova Scotia [22]. The conditions represent a typical flood tide when the mid-depth velocity ranged from 1.8 to 2 m/s.

The total velocity at the inlet was expressed as:

$$V(Y,t) = \bar{V}(Y) + v'(t) \quad (1)$$

where $\bar{V}(Y)$ is the mean velocity profile and $v'(t)$ is the turbulent component.

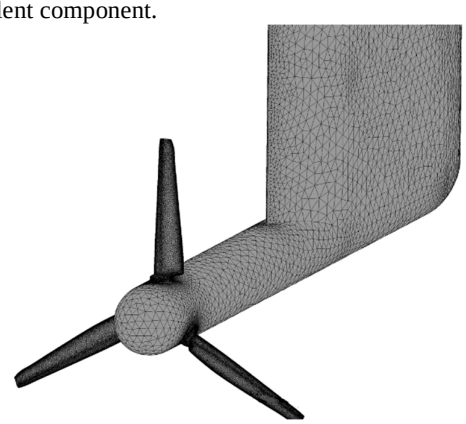

Fig. 3 Detailed view of turbine surface mesh.

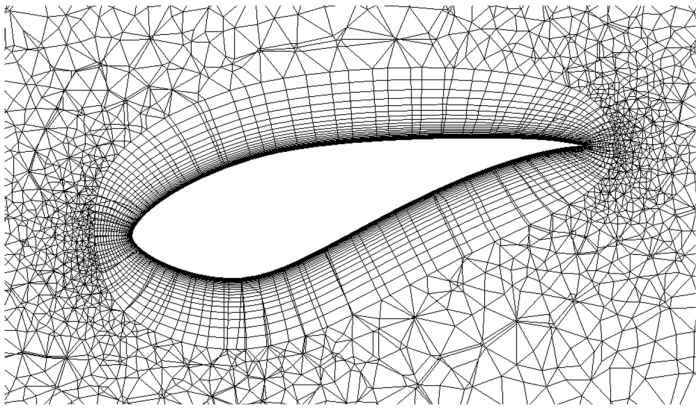

Fig. 4 Cross-section of the blade mesh.

TABLE IV
BOUNDARY CONDITIONS

Boundary	Condition
Inlet	Unsteady Flow with an Averaged Normal Velocity $\bar{V}$= 2.05 m/s
Outlet	P_{rel} = 0 Pa
Tank Walls	No-Slip, Side Wall Velocity = 2.05 m/s Top Surface as a Free Surface
Turbine Walls	No-Slip
Domain Interfaces	Transient Rotor

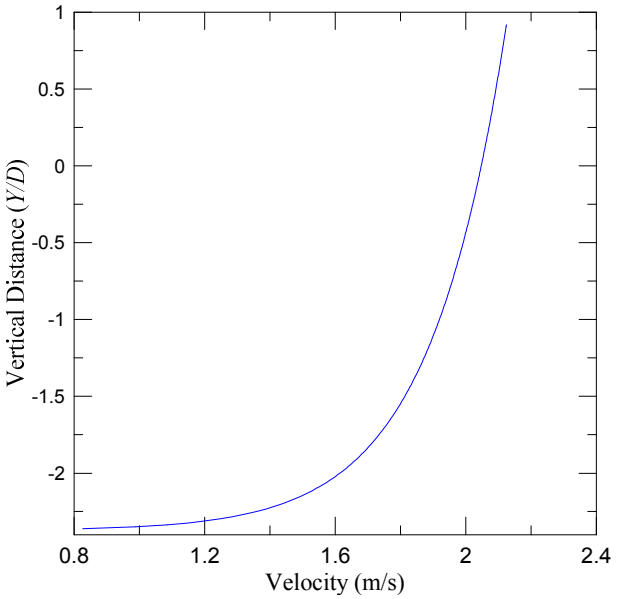

Fig. 5 Mean velocity profile $\bar{V}$ as a function of *Y*.

The mean velocity profile was generated from the law-of-the wall which is given by:

$$\bar{V}(Y) = \frac{v_*}{\kappa}\ln(\frac{Y}{Y_0}) \quad (2)$$

where $\kappa = 0.4$ is the von Karman constant, v_* is the friction velocity and Y_0 is the bottom roughness lengthscale. The v_* and Y_0 parameters are based on the best fit to the ADCP data and are given by v_* = 0.0939 m/s and Y_0 = 0.0037 m. The resulting velocity profile is shown in Fig. 5.

Because an ADCP cannot measure v' directly, the measured dissipation rate of ε = 8.6 × 10^{-5} W/kg was used to obtain a realistic turbulent velocity [22]. A synthetic time series was generated by superimposing waves of random phase at wavenumbers below the Kolmogorov microscale, where the amplitude of each Fourier component was such that the theoretical form of the spectral density, *S*, was ensured, *i.e.* $S \sim k^{-5/3}$. In reality, ε and hence v' varies with depth; however, in these initial simulations, v' was independent of *Y*. The 20 s synthetic time series of v' is plotted in Fig. 6 a).

No-slip conditions were applied to every surface in the model, except the top water surface which was simulated as a free surface. The side walls of the simulation domain were given the same average velocity as the inlet flow to limit the impact of the wall on flow dynamics. The rotational rate of the cylindrical domain was set to achieve the desired tip speed ratio (TSR), defined as:

$$TSR = \frac{\omega R}{\bar{V}} \quad (3)$$

where ω is the rotational rate in rad/s, *R* is the turbine radius (381 mm), and $\bar{V}$ is the reference velocity (constant during the experiment).

In addition, steady state simulations were performed in order to enable the comparison of the wake behaviour. These simulations used only the constant mean velocity profile $\bar{V}(Y)$ as inlet velocity. Two thousand iterations were necessary to reach convergence in the wake.

In these steady simulations, the frozen-rotor quasi-steady approach was used to model the dynamics of the flow (whereas the fully transient-rotor one was used for the transient runs). With the exception of the inlet velocity and the frozen- or transient-rotor approach, all the simulations were performed with the same mesh and boundary conditions. All simulations are performed at constant TSRs.

E. Resolution Procedure

All simulations were performed using between 26 and 30 cores on a Dell Precision T7810, 16 cores (2.4 GHz) hyper threaded with 128 GB of RAM. The computation time varied between 1 hour and 48hours (transient simulations).

IV. NUMERICAL COMPARISON BETWEEN UNSTEADY AND STEADY FLOW

A. Performance Calculation

Power and thrust coefficients are used for comparison. These properties are described as follows:

$$C_t = \frac{T}{\frac{1}{2}\rho A V_A^2} \quad (4)$$

$$C_p = \frac{P_m}{\frac{1}{2}\rho A V_A^3} = \frac{\omega Q}{\frac{1}{2}\rho A V_A^3} \quad (5)$$

where T and P_m are the thrust and mechanical power produced, respectively, ρ is the fluid density, A is the rotor swept area, and Q is the rotor torque.

Because a velocity profile is used at the inflow, velocity varies with depth. Depending on the choice of reference velocity made (mean velocity profile $\bar{V}$ averaged on a swept area, velocity $\bar{V}(Y)$ at a specific location Y_1, etc.), power and thrust coefficients values can differ substantially. As shown by Fleming *et al.*, the power curve may be misrepresented if an incorrect reference velocity is taken [29]. They showed that the correct reference velocity is the one equal to the integral of the velocity over the rotor swept area. Thus, for all thrust and power coefficients computed in this paper, $V_A(t)$ is defined as the integral over the velocity of the rotor swept area.

For the unsteady simulations, total velocity $V_A(t)$ is defined by:

$$V_A(t) = v'(t) + \overline{V_A} \quad (6)$$

Therefore $V_A(t)$ is given at time t_1. Due to the advection time of the fluid from the inlet to the turbine, the inflow velocity at t_1 does not correspond to the fluid's velocity going through the turbine at t_1. To determine the actual velocity at the turbine, a time offset has been added. This offset is equal to the advection time of the fluid from the inlet to the turbine equal to 0.75 s.

Figures 6 a), b) and c) show, respectively, the evolution of V, C_p and C_t as with time. In these figures, TSR is equal to 4 and the average velocity is set to 2.05 m/s. Twenty seconds of 'real data' were used to perform these simulations.

The magnitude of the fluctuations in the C_t is far higher than for C_p: C_p values varying from 0.24 to 0.4 whereas C_t values from 0.08 to 0.95.

This large variation in the C_t values (consequently, also in blade loading) could lead to an increase of the turbine/blade fatigue and stress, possibly reducing the life expectancy of the device.

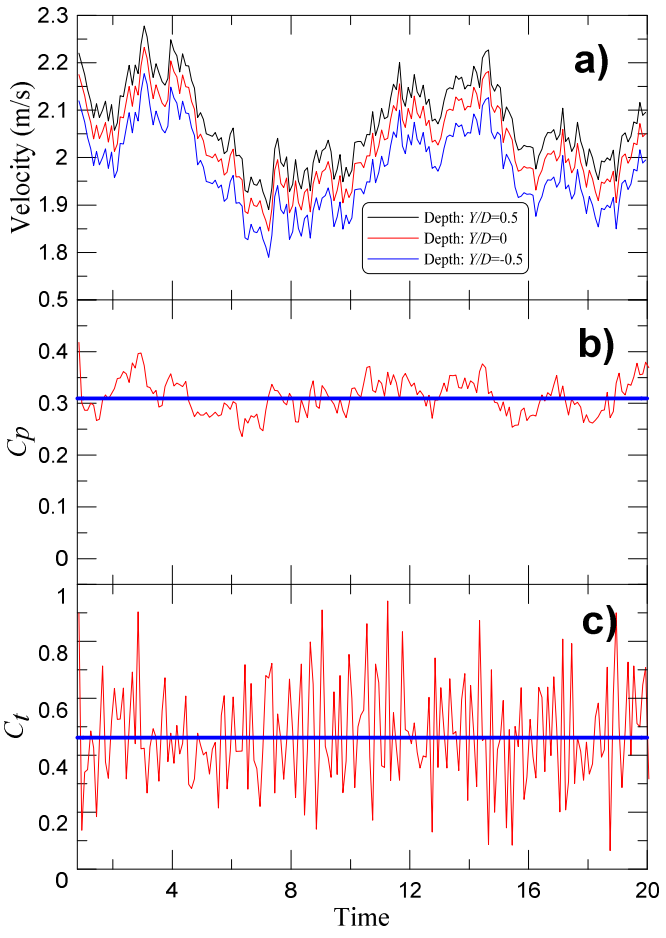

Fig. 6 a) Inlet Velocity as a function of time for 3 different depths: Y/D = 0.5, Y/D = 0 and Y/D = -0.5 (Y/D = 0 corresponds to the hub height) b) C_p, as a function of time and c) C_t as a function of time (blue: coefficient from the steady simulation, red from the transient one).

B. Power and Thrust Coefficients

With the inlet velocity being time-dependent in the transient simulations, the instantaneous velocity varies from 1.75 to 2.2 m/s (when the average velocity is 2.05 m/s). Therefore, for comparison, it was decided to perform the steady simulations with the same range of input speeds. Results in Fig. 7 include the results of steady simulations covering a range of tip speed ratios (TSR = 3 – 4.5) and velocities (1.75- 2.2 m/s). Transient simulations cover a range of TSR (3 - 4.5) obtained for one transient inlet velocity having an average of 2.05 m/s. Figure 7 shows the comparative C_p-TSR and C_t-TSR curves for steady and unsteady flow.

Both C_p and C_t follow a similar trend for steady and unsteady simulations. However, in the transient results, the fluctuation amplitude in the C_p and C_t values is much higher than for steady flow results.

The turbine's overall performance for an unsteady flow is comparable to the one obtained for a steady flow. The steady flow C_p curve has an average relative difference of 0.83% and average absolute difference of 0.003 below unsteady simulations values. Likewise, the predicted C_t curve has an average relative difference of 0.07% below unsteady simulations values. As can be seen, the relative difference grows with TSR to reach 0.5% for TSR=4.5.

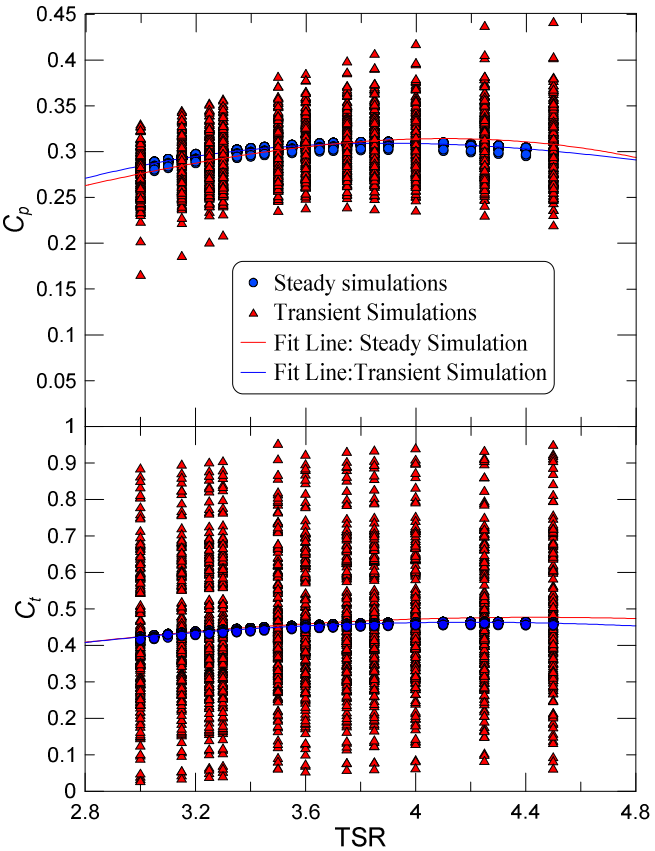

Fig. 7 C_p and C_t as a function of TSR.

V. Results and Discussion

A. Mechanical Performance

Following the presentation of results from Dr. Bjorn Elsaesser's group experiments [11], the mechanical performance of the turbine was assessed. To do so, new simulations were run with changed inlet conditions. Steady simulations covering a wider range of velocities (1.45 to 2.3 m/s) were performed at constant TSRs (3, 3.5 or 4), whereas in the transient simulations, three different velocities (integral of the velocity on the rotor swept area) were used: 1.6, 1.8 and 2.05 m/s. TSR remained constant for the duration of a simulation. The comparison of the mechanical power against inflow velocity for these three TSR-values is shown in Fig. 8.

In each case, the relationship between the mechanical power P_m and the velocity follows the power law expected from Eq. (5). The mechanical power is proportional to the power in the flow and thus the cube of the inflow velocity. The relationship is very consistent for the steady and unsteady flow even if the amount of scatter in the instantaneous P_m values is important for transient results.

Taking a closer look at the curves for each TSR, for TSR = 3.5, the unsteady tests mechanical performance is always lower than the steady one: approximately 7 W (3.3%) less than the steady tests at 1.45 m/s and 27.7 W (3.3%) less than the steady tests at 2.3 m/s. For TSR = 3 or 4, the difference between the steady and the transient mechanical performance depends on the velocity-value. For TSR = 3, the difference is close to 0 at 1.45 m/s and equal to 50 W (6.3%) and the opposite trend is seen for TSR = 4.

B. Wake Characteristics

Velocity deficit and turbulence intensity were computed in order to visualize what is happening in the wake, and are defined as:

$$V_{deficit} = 1 - \frac{V_W}{\bar{V}_A} \tag{7}$$

$$TI = \frac{100}{\bar{V}_A}\sqrt{\frac{2}{3}k} \tag{8}$$

where V_W is the local wake velocity and k is the turbulent kinetic energy. $\bar{V}_A$ is the time average of the integral of the velocity over the rotor swept area and therefore remains constant for the duration of the simulation (so no time offset was added to consider the advection time from the inlet to the turbine even for transient simulations).

To visualize clearly what is happening in the wake, dimensionless velocity (V/V_0) are plotted in Fig. 9 at different locations along the wake, both for steady and transient simulations. Because in transient simulations, the wake is constantly evolving, results only for a single specific time value are presented. This was chosen to be 20 s because it is a good compromise between the time needed to obtain a fully developed wake which can be observed to take approximately 10 s, and a simulation which lasts for too long.

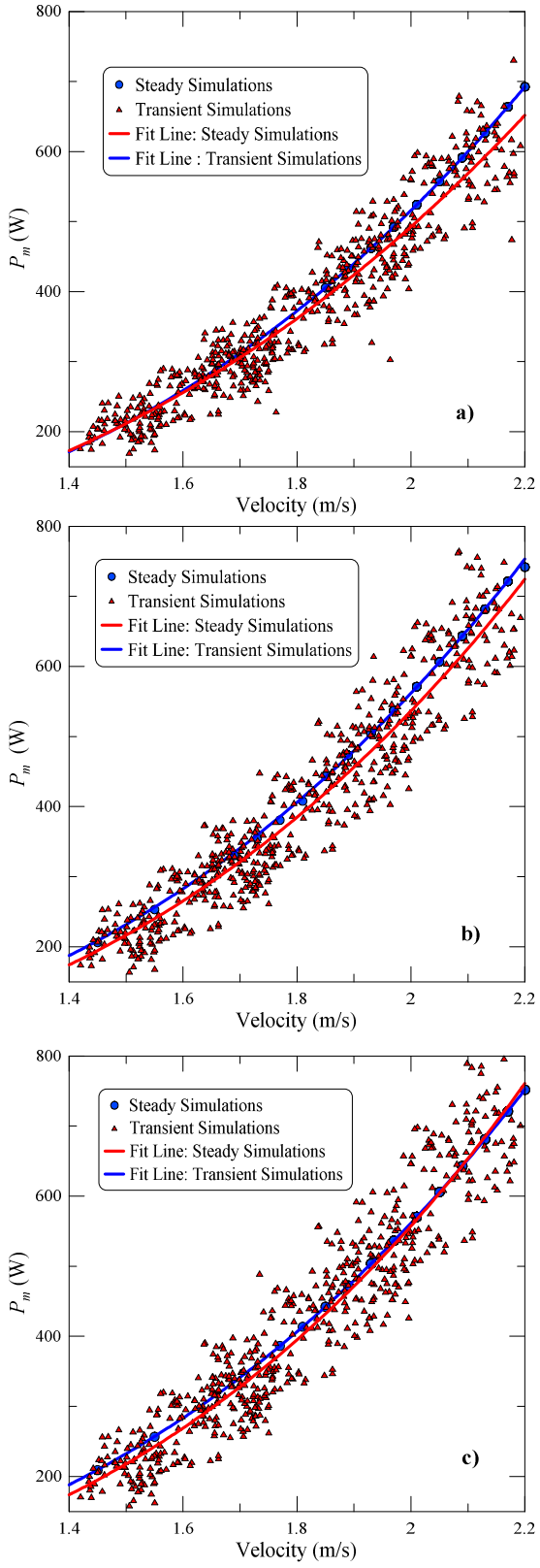

Fig. 8 Steady and transient mechanical power against inflow velocity for: a) TSR = 3, b) TSR = 3.5 and c) TSR = 4.

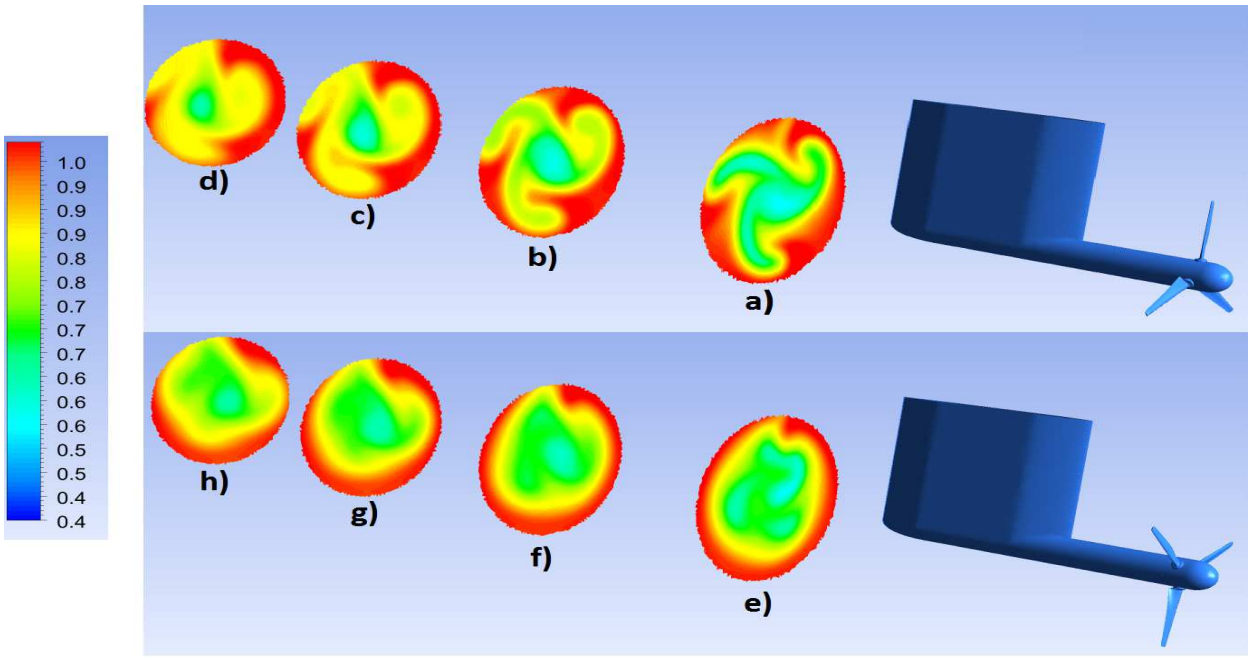

Fig. 9 Normalized Velocity V/V_0 for steady simulations at a) 3*D*, b) 5*D*, c) 7*D* and d) 9*D* and transient simulations at e) 3*D*, f) 5*D*, g) 7*D* and h) 9*D*.

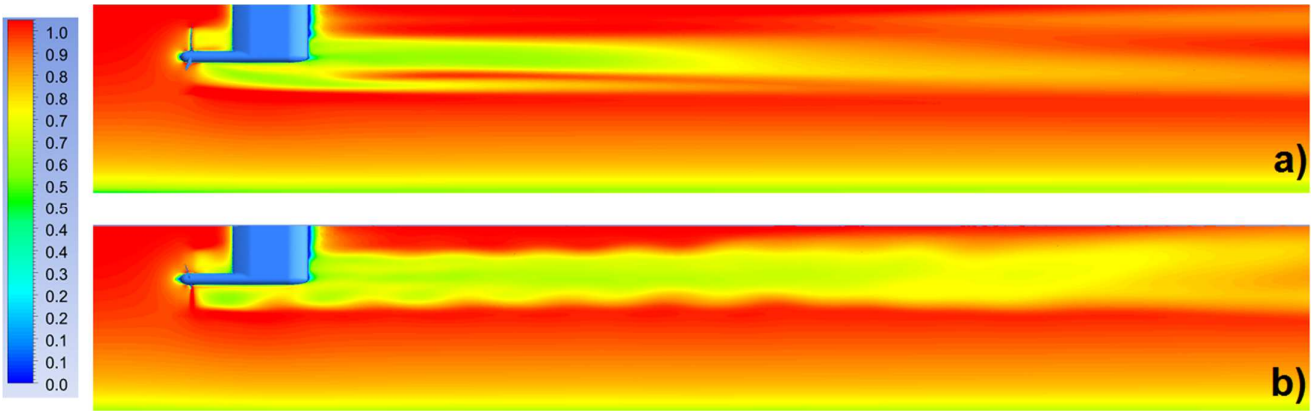

Fig. 10 Normalized Velocity V/V_0 on mid-vertical plane for a) steady flow, b) transient flow at t = 20 s.

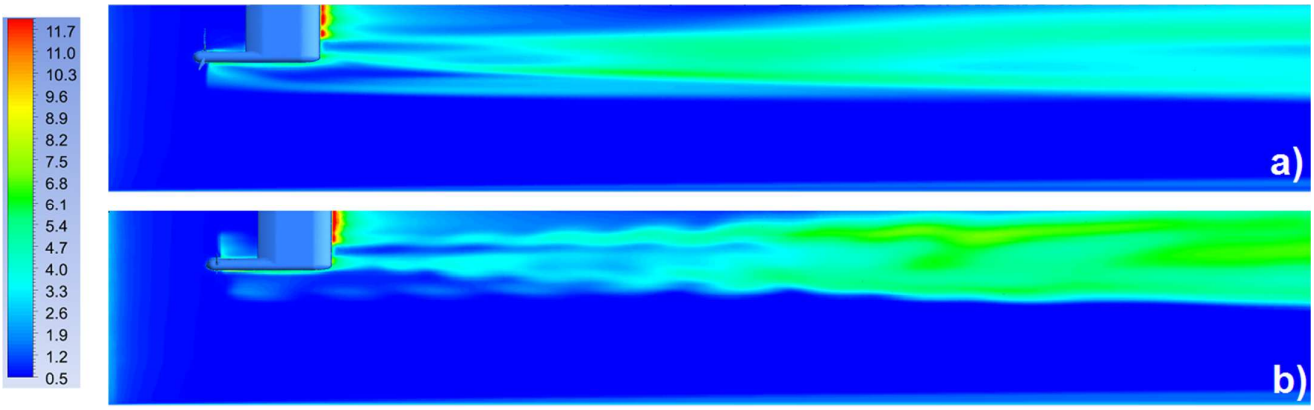

Fig. 11 Turbulence intensity on mid-vertical plane for a) steady flow, b) transient flow at t = 20 s.

The shape of velocity profile through the wake is different: a cylindrical-shaped wake for transient flow whereas there is a "turbine-shaped" wake for steady simulations. Moreover, the velocity deficit seems to disappear faster in the constant velocity simulations. Figure 9 a), b), c) and d) also illustrates the effects, of the fixed rotor blades in the steady simulation. In contrast, in transient simulations, with the Transient Rotor approach, the blades are always moving. That is why a large circle profile can observe in the transient simulation.

Figure 10 represents the normalized velocity on mid-vertical plane. It shows that the velocity deficit is more important for transient simulations in the far field wake (7*D* and 9*D*) but it is the opposite in the near field. As mentioned earlier, depending on the type of inflow velocity used, the shape of the wake is different. The wake is wider for the turbulent simulation and disappears more slowly. At a distance of 10*D*, velocity is approaching the inflow velocity for steady state whereas the velocity deficit is still important in the second case. Even at a distance of 20*D*, the flow is still affected by the turbine in the transient case.

Figure 11 presents the turbulence intensity along the centre plane of the wake. Unlike velocity profiles, turbulence intensity profiles are much the same in both cases: turbulence is still significant at a distance of 20*D* and increases as moving away from the turbine. When turbulence intensity is lower than 4% in the near wake, it is approximately 6% at a distance of 20*D*. As above, turbulence is higher in the transient case, especially in the far wake: at a distance of 20*D*, maximum turbulence intensity is 3.6% for constant flow simulations and 5.7% for the unsteady simulation. This may due to the large fluctuation of the inlet velocity during the simulation.

Figures 12 and 13 present the values of turbulence intensity and velocity deficit over horizontal lines and vertical lines at 5*D*, 10*D*, 15*D* and 20*D*. First, both for velocity deficit and turbulence intensity, there is no symmetry along *Z*. In steady simulation, this is due to the Frozen Rotor approach which forces the fluid to twist around the blades. That twist is always generated in the same side of the blade and thus it creates a deflection at *X/D*= -0.5 as seen in Figs. 12 and 13 b)-c)-d). At 5*D*, irregularities in the turbulence intensity can be observed at *x*/*D* = 0 and ± 0.5 (especially in the transient simulations). These irregularities correspond to the turbulence due to root and tip losses, and nacelle structure interaction.

Regarding the velocity deficit, the wake seems to become wider from 5*D* to 20*D*, both in the horizontal and vertical directions. The velocity deficit is not confined anymore between -0.5 and 0.5 m (in both directions at 5*D*) but between -0.75 and 0.9 m (vertical direction at 20*D*). The results demonstrate also that average velocity deficit is higher in the transient simulations than steady simulations and so the velocity deficit disappears faster in the constant velocity simulations. For example, the average velocity deficit is approximately 0.09 at a horizontal distance of 10*D* for a constant velocity inflow and 0.15 for transient simulations. However, velocity deficit in constant velocity simulations seems to be over-predicted outside of the wake.

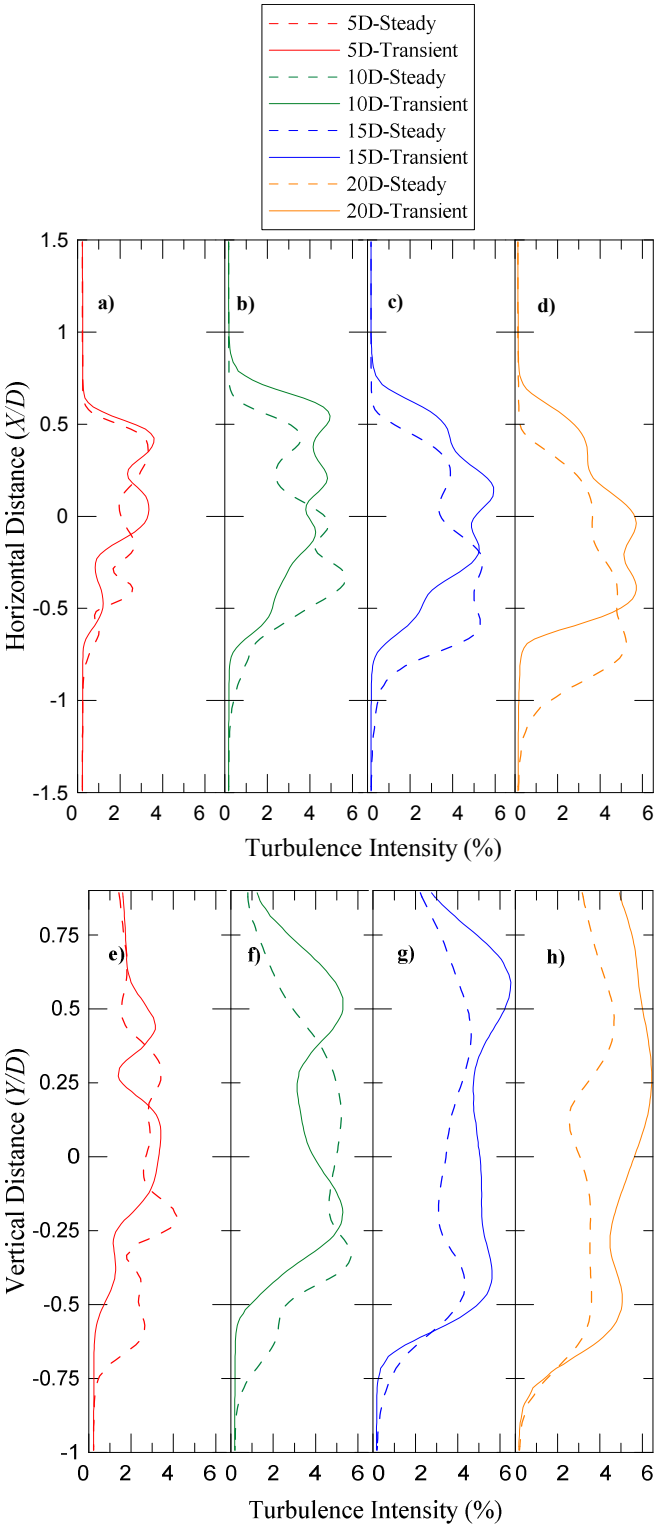

Fig. 12 Turbulence intensity: a) Horizontal - 5*D*, b) Horizontal - 10*D*, c) Horizontal - 15*D*, d) Horizontal - 20*D*, e) Vertical - 5*D*, f) Vertical - 10*D*, g) Vertical - 15*D*, h) Vertical - 20*D*.

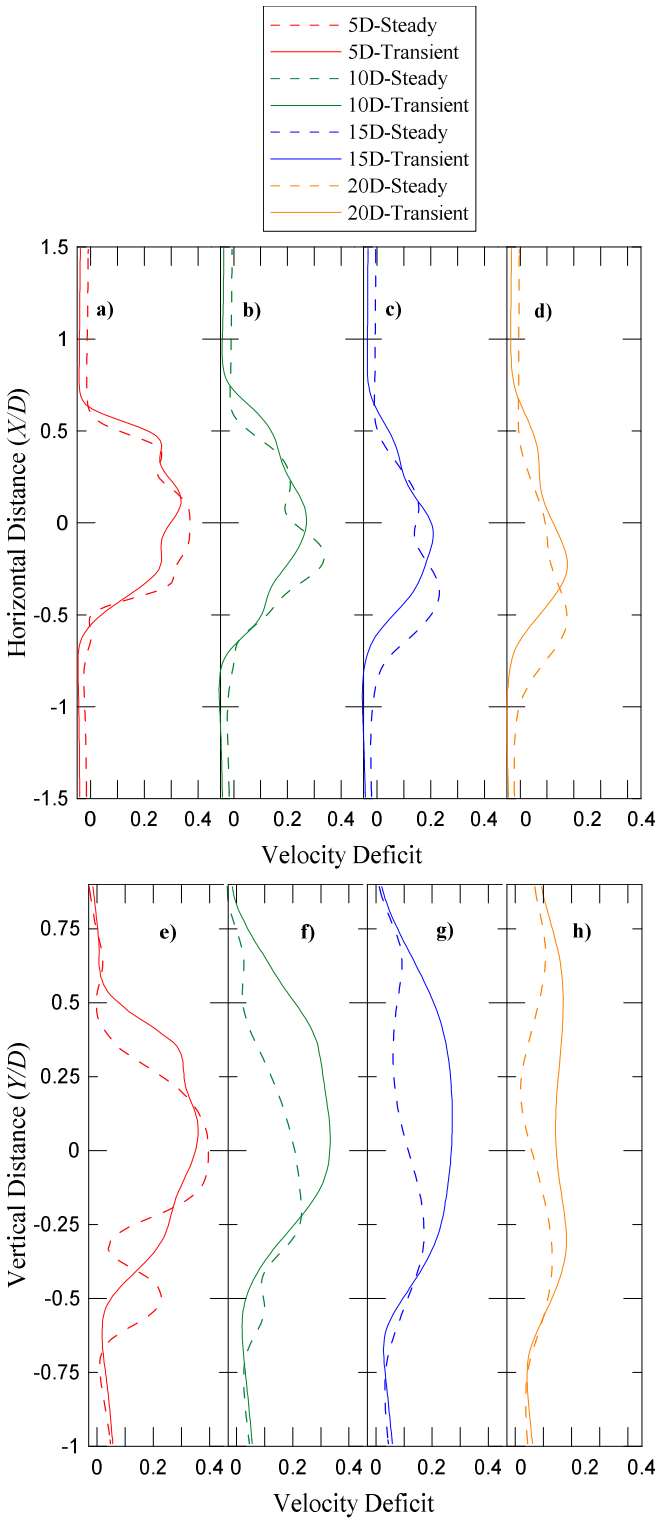

Fig. 13 Velocity deficit: a) Horizontal - 5*D*, b) Horizontal - 10*D*, c) Horizontal - 15*D*, d) Horizontal - 20*D*, e) Vertical - 5*D*, f) Vertical - 10*D*, g) Vertical - 15*D*, h) Vertical - 20*D*.

Regarding turbulent intensity, results may be difficult to interpret: for turbulence intensity as a function of vertical distance, turbulence is higher for transient results than steady one. For instance, at a distance of 15*D*, average turbulence intensity is approximately 3% for steady state simulations and 4% for transient. However, it is not so obvious when looking to turbulence as a function of horizontal distance *e.g.* at a distance of 20*D*, average turbulence intensity is equal to 1.7% for transient flow and 1.9% for steady flow simulations. It can also be seen that turbulence increases from 5*D* to 20*D* in both directions.

VI. Conclusions

A numerical model of a three bladed horizontal axis tidal turbine under realistic turbulent tidal flow has been created. The preliminary results of this investigation have been compared with steady flow numerical model results with good agreement in trends. Prediction of both C_p and C_t are very similar in both cases. These similar trends observed in both C_p and C_t curve are important as they indicate that the appropriate flow physics are being accounted for. Only TSR values related to maximum C_p and C_t changed. For C_p curves, tip speed ratio is approximately equal to 3.9 in steady flow and 4.1 for transient conditions. In transient flows, this results however in an approximate 4% reduction in performance (for TSR = 3.5), though there is increased uncertainty due to the levels of scatter in the numerical data points.

Velocity deficit plots show the wake is wider in transient simulations than steady ones. The velocity deficit disappears also faster in the constant velocity simulations. Turbulent effects in the wake seem to increase after a distance of 10*D* downstream of the turbine in this setup, as shown in Fig. 13. These turbulence effects are higher in the transient simulations.

This comparative analysis of numerical steady and transient simulations shows the impact of the unsteadiness of realistic tidal flows on the performance of tidal turbines. In view of the above, the current use of steady state testing (numerical or experimental) for design stage can be questioned. The observed changes in the wake's characteristics and the high variations of the loads on the blades (reference to *Ct*-curve as a function of time) must also be better assessed.

Acknowledgment

The authors are grateful to the Offshore Energy Research Association (OERA) of Nova Scotia and the Canadian Foundation for Innovation (CFI) for their financial support for this work.

References

[1] (2014) The Marine Current Turbines website. [Online]. Available: http://www.marineturbines.com/

[2] (2016) The Atlanted Resources website [Online]. Available: http://atlantisresourcesltd.com/marine-power/global-resources.html

[3] J. McNaughton, S. Harper, R. Sinclair, B. Sellar, "Measuring and Modeling the Power Curve of a Commercial-Scale Tidal Turbine" in *The 11th European Wave and Tidal Energy Conference*, 2015.

[4] A. S. Bahaj, A.F. Molland, J.R. Chaplin, W.M.J. Batten, "Power and thrust measurements of marine current turbines under various hydrodynamic flow conditions in a cavitation tunnel and a towing tank" in *Renewable Energy*, 32, pp. 407-426, 2007.

[5] D. Doman, R.E. Murray, M.J. Pegg, K. Gracie, C.M. Johnstone, T. Nevalainen, "Tow-tank testing of a 1/20th scale horizontal axis tidal turbine with uncertainty analysis" in *International Journal of Marine Energy*, 11 pp. 105-119, 2015.

[6] P. Mycek, B. Gaurier, G. Germain, G. Pinon, E. Rivoalen, "Experimental study of the turbulence intensity effects on marine current turbines behavior. Part I: one single turbine" in *Renewable Energy*, 66, pp. 729-746, 2014.

[7] W.M.J. Batten, A.S. Bahaj, A.F. Molland, J.R. Chaplin, "The prediction of the hydrodynamic performance of marine current turbines" in *Renewable Energy*, 33, pp. 1085-1096, 2014.

[8] A. S. Bahaj, W.M.J. Batten, G. McCann, "Experimental verifications of numerical predictions for the hydrodynamic performance of horizontal axis marine current turbines" in *Renewable Energy*, 32, pp. 2479-2490, 2007.

[9] M.E. Harrison, W.M.J. Batten, L.E. Myers, A.S. Bahaj, "A comparison between CFD simulations and experiments for predicting the far wake of horizontal axis tidal turbines" in *The 8th European Wave and Tidal Energy Conference*, 2009.

[10] C.H. Jo, J.H. Lee, Y.H. Rho, K.H. Lee, "Performance analysis of a HAT tidal current turbine and wake flow characteristics" in *Renewable Energy*, 65, pp 175-182, 2014.

[11] P. Jeffcoate, B. Elsaesser, T. Whittaker and C. Boake, "Testing Tidal Turbine – Part 1: Steady Towing Tests vs. Tidal Mooring Tests" in *International Conference on Offshore Renewable Energy*, 2014.

[12] P. Muller, F. Sainclair, A. Carlisle, C. Delafosse, "Tidal Current Turbine Optimization using CFD Simulation" in the *11th European Wave and Tidal Energy Conference*, 2015.

[13] J.H. Lee, S. Park, D.H. Kim, S.H. Rhee, M.-C. Kim, "Computational methods for performance analysis of horizontal axis tidal stream turbines" in *Applied Energy*, 98, pp. 512-523, 2012.

[14] T. O'Doherty, A. Mason-Jones, D.M. O'Doherty, C.B. Byrne, I. Owen, Y.X. Wang, "Experimental and Computational Analysis of a Modal Horizontal Axis Tidal Turbine" in *The 8th European Wave and Tidal Energy Conference*, 2009, p. 1085-1096.

[15] R. McSherry, J. Grimwade, I. Jones, S. Mathias, A. Wells, A. Mateus, "3D CFD modelling of tidal turbine performance with validation against laboratory experiments" in *The 9th European Wave and Tidal Energy Conference*, 2011.

[16] U. Ahmed, I. Afgan, D.D. Apsley, T. Stallard, P.K. Stansby, "CFD Simulations of a Full-Scale Tidal Turbine: Comparison of LES and RANS with Field Data" in *the 11th European Wave and Tidal Energy Conference*, 8p, 2015.

[17] X. Wang, A.H. Day, "CFD Turbulence Modelling of Tidal Turbine Unsteady Blade Load" in *the 11th European Wave and Tidal Energy Conference*, 10 p., 2015.

[18] T. Blackmore, B. Gaurier, L. Myers, G. Germain, A.S. Bahaj, "The Effect of Freestream Turbulence on Tidal Turbines" in *the 11th European Wave and Tidal Energy Conference*, 8 p., 2015.

[19] P. Mycek, B. Gaurier, G. Germain, G. Pinon, E. Rivoalen, "Experimental study of the turbulence intensity effects on marine current turbines behavior. Part II: two interacting turbines" in *Renewable Energy*, 68, pp. 876-892, 2014.

[20] A.E. Hay, J. McMillan, R. Cheel, D. Schillinger, "Turbulence and Drag in a High Reynolds Number Tidal Passage targeted for In-stream Tidal Power" in the *IEEE Oceans'13*, 2013.

[21] J.M. McMillan, A.E. Hay, R.G. Lueck, and F. Wolk, "An Assessment of the Dissipation Rates at a Tidal Energy Sites using a VMP and an ADCP", in the *11th European Wave and Tidal Energy Conference*, 8 p, 2015.

[22] J.M. McMillan, A.E. Hay, R.G. Lueck, and F. Wolk, "Rates of dissipation of turbulent kinetic energy in a high Reynolds number tidal channel" in Journal of Atmospheric and Oceanic Technology, 33, pp 817 -- 837, 2016.

[23] K.W. Wilcox, I. McLeod, A. Gerber, T. Jeans, J. Culina, "Validation of High-Fidelity CFD Simulation of the Unsteady Turbulent Tidal Flow in Minas Passage" in the *11th European Wave and Tidal Energy Conference*, 13 p, 2015

[24] N. Osbourne, D. Groulx, and I. Penesis,"3D Modelling of a tidal turbine – a numerical investigation of wake phenomena" in *the 11th European Wave and Tidal Energy Conference*, 10p, 2015.

[25] F. Menter, "Tow-equation eddy-viscosity turbulence models for engineering applications" in *AIAA Journal*, pp. 1598-1605, 1994.

[26] I. Afgan, J. McNaughton, S. Rolfo, D.D. Apsley, T. Stallard, P. Stansby, "Turbulent flow and loading on a tidal stream turbine by LES and RANS" in *International Journal of Heat and Fluid Flow*, pp. 96-108, 2013.

[27] J. McNaughton, S. Rolfo, D. Apsley, I. Afgan, T. Stallard, P. Stansby, "CFD Prediction of Turbulent Flow on an Experimental Tidal Stream Turbine using RANS modelling" in *The 1st Asian Wave and Tidal Energy Conference Series*, 2012.

[28] G. Currie, N. Osbourne and D. Groulx, "Numerical Modelling of a Three-Bladed NREL S814 Tidal Turbine" to be published and presented at AWTEC 2016 in October 2016.

[29] C.F. Fleming, S.C. McIntosh, R.H.J. Willden, "Tidal turbine performance in sheared flow" in *The 10th European Wave and Tidal Energy Conference*, 2013.